





Article

Optimization Study of CO₂ Gas Absorption with NaOH Absorbent Continuous System in Raschig Ring Packing Column Using Box–Behnken Design

Jakfar ^{1,*}, Husni Husin ^{1,2}, Muhammad Zaki ¹, Lia Mairiza ^{1,2}, Mirna Zulrika ¹, Fahrizal Nasution ^{1,2} and Ahmadi ¹

¹ Chemical Engineering Department, Engineering Faculty, Universitas Syiah Kuala, Darussalam, Banda Aceh 23111, Indonesia; husni_husin@che.unsyiah.ac.id (H.H.); m.zaki@unsyiah.ac.id (M.Z.); liamairiza@usk.ac.id (L.M.); mirna63@mhs.unsyiah.ac.id (M.Z.); fahrizalnasut@gmail.com (F.N.); ahmadiahmadi840@gmail.com (A.)

² Doctoral Program, School of Engineering, Universitas Syiah Kuala, Darussalam, Banda Aceh 23111, Indonesia

* Correspondence: jakfar@che.unsyiah.ac.id

Abstract: Increasing CO₂ gas emissions results in climate change by increasing air temperature and worsening environmental problems. It is necessary to control CO₂ gas in the air to overcome this. This research aims to optimize the absorption of CO₂ gas in the air with 0.1 M NaOH absorbent in the tower of the Raschig ring stuffing material using the response surface methodology (RSM). This research was conducted using a continuous system of three independent variables by varying the contact time (10–80 min), the flow rate of NaOH absorbent (2–5 L/min), and the flow rate of CO₂ gas (1–5 L/min). The response variables in this study were the absorption rate (L/min) and mass transfer coefficient, while the air flow rate was constant at 20 L/min. Air and CO₂ gas mix before absorption occurs and flow into the Raschig ring packing column so that contact occurs with the NaOH absorbent. Mass transfer of CO₂ gas occurs into the NaOH absorbent, resulting in absorption. The results showed that the effect of contact time (min), the flow rate of NaOH absorbent (L/min), and CO₂ gas flow rate individually and the interaction on CO₂ absorption rate and mass transfer coefficient were very significant at a *p*-value of 0.05. Chemical absorption of CO₂ also occurred due to the reaction between CO₂ and OH[−] to form CO₃^{2−} and HCO₃[−], so the pH decreased, and the reaction was a function of pH. Optimization using Design Expert 13 RSM Box–Behnken Design (BBD) yielded optimal conditions at an absorption time of 80 min, NaOH absorbent flow rate of 5 L/min, CO₂ gas flow rate of 5 L/min, absorption rate of CO₂ gas of 3.97 L/min, and CO₂ gas mass transfer coefficient of 1.443 mol/min m² atm, with the desirability of 0.999 (≈100%).

Keywords: absorption; Box–Behnken design; carbon dioxide; response surface methodology; optimization



Citation: Jakfar; Husin, H.; Zaki, M.; Mairiza, L.; Zulrika, M.; Nasution, F.; Ahmadi Optimization Study of CO₂ Gas Absorption with NaOH Absorbent Continuous System in Raschig Ring Packing Column Using Box–Behnken Design. *Inventions* **2023**, *8*, 70. <https://doi.org/10.3390/inventions8030070>

Academic Editor: Rahmat Ellahi

Received: 11 April 2023

Revised: 4 May 2023

Accepted: 6 May 2023

Published: 9 May 2023



Copyright: © 2023 by the authors. Licensee MDPI, Basel, Switzerland. This article is an open access article distributed under the terms and conditions of the Creative Commons Attribution (CC BY) license (<https://creativecommons.org/licenses/by/4.0/>).

1. Introduction

Air pollution and climate change have become major challenges for sustainable development related to CO₂ emissions [1]. Environmental degradation caused by various human activities, especially CO₂ emissions, is responsible for many disasters around the world, such as prolonged droughts, fires, tsunamis, and floods [2]. Increased CO₂ emissions cause severe environmental problems, such as climate change and melting glaciers [3,4], and are predicted to continue to increase, reaching a peak in 2030 [5]. Various alternative ways of CO₂ control proposed for the development include converting CO₂ into chemicals [6,7]. They comprehensively explored the factors that contribute to CO₂ uptake by nanofluids, mainly addressing the role of base fluids and the reasons for their choice was reported by (Aghel et al., 2022) [8]. Utilization of CO₂ is for catalytic conversion [9], electrocatalytic

reduction [10], photocatalytic reduction [11], thermocatalysis, green hydrogen from renewable energy sources, and transformation of CO₂ into materials [12–14]. However, managing air pollution and greenhouse emissions has not achieved the expected synergistic results.

Researchers call for coordinated efforts to improve air quality and combat climate change [15]. The adverse effects of CO₂ emissions are felt by developed countries (G7) [16]. Indicators of climate change include heat waves, floods, droughts, and heavy rainfalls. To prevent such a calamity, the United Nations Framework Convention on Climate Change established an international environmental agreement to restrict the average global temperature increase to <2 °C. Lowering CO₂ emissions is a response to climate change because greenhouse gas buildup alters the atmosphere and captures solar energy at the earth's surface. CO₂ is released in various circumstances, including the combustion of oil, coal, gas, petroleum, petrochemicals, and deforestation [17].

(Tollefson, 2017) [18], asserts that if greenhouse gases remain elevated, global temperatures will rise by 5–6 °C by the end of the century. This warning was reiterated in the results of the Glasgow Climate Pact (COP26), which stated that climate regulators will need to achieve net-zero emissions by 2050 through significant decreases in emissions of greenhouse gases. The gradual rise in climate-related dangers has spurred nations to shift the modes of development of existing economies in a low-carbon direction [16,19] and build tactics to lower carbon emissions and advance the Paris Agreement's objectives [20]. As a result, 190 parties have ratified the Paris Agreement as of January 2021, pledging to develop a low-carbon economy. However, in their pursuit of low-carbon development, nations confront a paradox: energy is a crucial driver of economic development, but fossil energy has a negative impact on the environment and contributes to greenhouse gas emissions [21,22].

The environmental challenges faced are how to produce safer and less expensive energy while reducing greenhouse gas emissions [23]. Solving this challenge requires finding alternative energy sources and capturing CO₂ gas [24,25]. The primary sources of global warming are greenhouse gases, with carbon dioxide having the most significant impact [26,27]. The problems caused by global warming include an increase in natural disasters, a rise in sea level, desertification, and biodiversity loss, all of which pose a grave threat to human life and development [26,27]. A study by Sharma et al., 2023 reported on the enhanced electron transfer and ion diffusion from the unique MgV and graphene oxide. The MgV/reduced graphene oxide composite delivers excellent capability in the detection of sulfadiazine in real samples of human blood serum [28]. More than one hundred countries have signed the Kyoto Protocol, whose primary objective is to reduce carbon emissions in order to safeguard humanity from the peril of global warming. The long-term objective of the Paris Agreement of 2016 is to keep global average temperature increases to less than 2 °C above pre-industrial levels and to work toward limiting temperature increases to 1.5 °C above pre-industrial levels. To support the reduction of greenhouse gas emissions as the primary cause and have the most significant impact, specifically regarding CO₂ gas [26,27], this research concentrates on reducing CO₂ through the absorption process in the packing tower and optimization via RSM BBD.

The difference in the research that has been carried out lies in the materials, chemical composition, operating conditions, desired target, capacity, tools used for the application, and optimization. Several studies are listed in Tables 1 and 2.

Multi-purpose optimization methods are widely used to support decision-makers in overcoming problems with different objectives, from one side wanting to obtain the maximum benefit and the other side preserving the environment and promoting sustainable development. However, with increasingly stringent global CO₂ emission laws, we face the challenge of balancing conflicting commercial and environmental objectives simultaneously [17,26,27]. This research optimizes CO₂ gas tower filling materials using Raschig ring and absorbent NaOH 0.1 M. The studied attributes are flooding, absorption rate, CO₂ gas mass contraction coefficient, and optimal conditions.

Table 1. Flue gas composition typical of a real coal-fired power plant and the intended industrial incinerator unit.

Coal-Fired Power Plant		Target Industrial Incinerator Unit
Temperature	160–180 °C	70 °C
Pressure	1 atm	1 atm
H ₂ O	20–23 (vol. % wet)	30 (vol. % wet)
CO ₂	10–11 (vol. % wet) 12.5–114.5 (vol. % dry)	5–11 (vol. % dry)
O ₂	4–5 (vol. % wet) 5.0–6.5 (vol. % dry)	8–12 (vol. % dry)
SO ₂	129–200 (wet ppm volume) 260–457 (dry mg/m ³)	6.2 (dry mg/m ³)
NO _x	150–250 (wet ppm volume) (≈99%) 237–410 (dry mg/m ³)	1.399
NO. balance NO ₂ and N ₂ O		

Table 2. Pilot for CO₂ capture from flue gas and using MEA-based technology.

Research Group		Flue Gas Source	CO ₂ Production	Columns Dimensions	References
Institute of Thermodynamics and Thermal Process Engineering	University of Stuttgart, Germany	Natural gas burner	10 kg CO ₂ /h	Absorption: H = 4.2 m; Ø = 0.125 m Stripper: H = 2.55 m; Ø = 0.125 m	[29,30]
SINTEF-NTNU	NTNU, Trondheim, Norway	Gas reconstituted	10 kg CO ₂ /h	Absorption: H = 4.3 m; Ø = 0.15 m Stripper: H = 3.9 m; Ø = 0.1 m	[31,32]
International Test Centre for CO ₂ Capture (ITC)	University of Regina, Canada	Natural gas burner	1 ton CO ₂ /day	Absorption: H = 10 m; Ø = 0.33 m Stripper: H = 10 m; Ø = 0.33 m	[33,34]
Projet SOLVit (SINTEF, NTNU, Aker clean carbon)	SINTEF, Trondheim, Norway	Not mentioned	1 ton CO ₂ /day	Absorption: H = 19 m; Ø = 0.2 m Stripper: H = 13.6 m; Ø = 0.162 m	[35]
Luminant Carbon Management Program	University of Texas at Austin, USA	Gas reconstituted	4 ton CO ₂ /day	Absorption: H = 13.3 m; Ø = 0.43 m Stripper: H = 13.3 m; Ø = 0.43 m	[36,37]
Nanko pilot KEPCO and MHI	Osaka, Japan	Natural gas turbine	2 ton CO ₂ /day	Not mentioned	[38,39]
International Test Centre for CO ₂ Captage (ITC)	Boundary Dam, Canada	Coal-fired power plant	4 ton CO ₂ /day	Absorption: Ø = 0.46 m Stripper: Ø = 0.40 m	[33]
Projet CASTOR and projet CESAR	Esbjervaerket, Denmark	Coal-fired power plant	24 ton CO ₂ /day	Absorption: H = 17 m; Ø = 1.1 m Stripper: H = 10 m; Ø = 1.1 m	[34,40]
IFPEN ENEL	Brindisi, Italy	Not mentioned	54 ton CO ₂ /day	Not mentioned	[41]

2. Materials and Methods

2.1. Materials

NaOH (Merck), HCl (Merck), phenolphthalein indicator, methyl orange, distilled water, and CO₂ gas in cylinders purchased by order from PT Aneka Gas in Medan City, North Sumatra Province, Indonesia.

2.2. Experimental

The equipment used included a filling absorption tower consisting of a glass column, packing material (packing) Raschig ring type glass, absorbent pump, air compressor, regulator, and flow meter for absorption. CO₂ gas cylinders were used, complete with pressure regulators and supporting equipment, namely pH meters, Dosimat 632, beakers, measuring cups, and pipettes. The working method was changing the pressure drop (P) in dry and wet conditions; filling in flooded conditions; filling absorbed and non-absorbed

gas in glass; and using chemical means by varying the flow rate of CO₂ gas and air, then mixing them. Two gas variations in the flow rate of 0.1 M NaOH absorbent, height, and diameter of the packing ring on a fixed column were used. The response variables were the absorption rate and mass contraction coefficient. The experimental design tested the effect of each variable, the effect of interaction, and optimization using Design Expert 13, Response Surface Methodology, Box–Behnken Design (RSM-BBD), and subtype random. A series of equipment using an absorption column was located in the Chemical Engineering Laboratory, Faculty of Engineering, Syiah Kuala University. The schematic procedure of the CO₂ gas absorption process using 0.1 M NaOH absorbent in the packing Raschig ring column is shown in Figure 1.

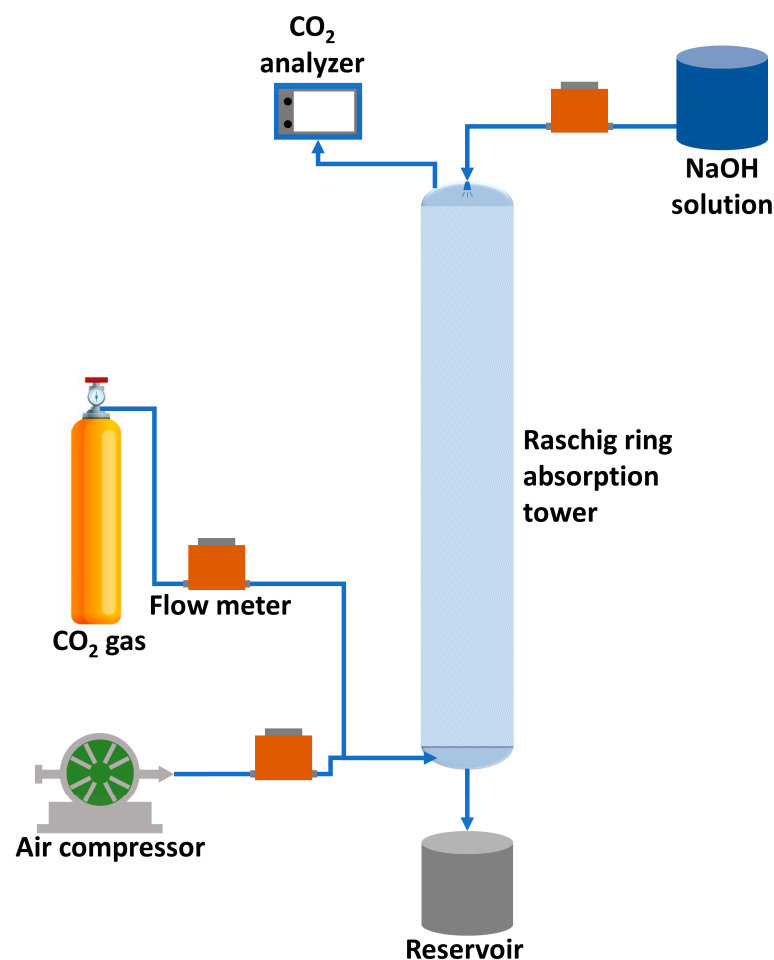


Figure 1. Schematic procedure of the CO₂ absorption process using 0.1 M NaOH absorbent in the Raschig ring packing column.

2.2.1. Calculation Principles Used

$$\text{CO}_2 \text{ volume fraction, } Y_o = \frac{V_2}{V_1} \quad (1)$$

Y_o is the mole fraction of CO₂ gas that is not absorbed; for the ideal gas fraction volume, it is the same as the mole fraction. From the incoming gas, the gas (air) flow rate enters (F_2), and the CO₂ flow rate enters (F_3) so that the mole fraction of gas entering [42]:

$$Y_1 = \frac{F_3}{F_2 + F_3} \quad (2)$$

If the F_a of CO_2 gas is absorbed (L/s), then

$$[F_2 + F_3]Y_i - [F_2 + (F_2 + F_a)]Y_0 = F_a \quad (3)$$

From Equations (2) and (3), we obtain:

$$F_a = \frac{(Y_i - Y_0)(F_2 + F_3)}{1 - Y_0} = \frac{(Y_i - Y_0)}{(1 - Y_0)}(F_2 + F_3) \quad (4)$$

To convert the absorbed CO_2 flow rate, F_a (L/s) to G_a (gmol/s) [43–46]:

$$G_a = \frac{F_a}{22.42} \left(\frac{P_{av}}{760} \right) \left(\frac{273}{T_{av} + 273} \right) \quad (5)$$

2.2.2. Determination of the Overall Mass Transfer Coefficient (k_{og}) [42,43]

The overall mass transfer coefficient, which controls the rate at which reactants and products are moved between the gas and liquid phases, is a crucial metric to compute in the conversion of CO_2 . This parameter impacts the mass transit rate of CO_2 from the gas phase to the liquid phase and the rate of CO_2 absorption into a liquid solvent in the context of CO_2 conversion.

The general equation used for absorption is presented in Equation (6):

$$H = \int_{Y_i}^{Y_0} \frac{d(G.Y)}{k_{og}.a.A(Y^* - Y)} \quad (6)$$

where:

Y^* = the mole fraction of the gas in equilibrium with the liquid at some point in the tower

Y = bulk mole fraction

A = tower cross-sectional area

H = height of the infill material in the tower

a = specific area of the stuffing material/unit volume of the stuffing material

The right-hand side is difficult to determine, so it can be determined more thoroughly as follows:

$$N = k_{og} (a.A.H) \log \text{average driving force pressure drop [46–50].}$$

where:

N = absorption rate (gmol/s)

A = column cross-sectional area

H = tower height

AH = column volume

$a.A.H$ = mass transfer area

So that:

$$k_{og} = \frac{N}{a.A.H} \left(\frac{\ln \frac{p_i}{p_o}}{p_i - p_o} \right) \quad (7)$$

where:

p_i = partial pressure of incoming CO_2 gas

p_o = partial pressure of outgoing CO_2 gas

2.2.3. Determination of Absorption of CO_2 Based on Chemical Reactions

The CO_2 is absorbed by the standard NaOH solution, and the normality of the solution will be affected. A mixture of carbonates and bicarbonates can be determined by titration with standard acid solutions using phenolphthalein and methyl orange indicators. The

carbonate ion is usually titrated as a base with a strong acid, resulting in a reaction as shown in Equations (8) and (9). In Table 3, ions formed at various temperatures are enumerated.

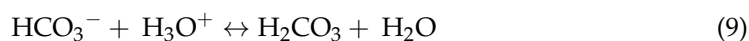
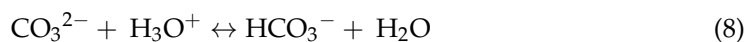


Table 3. Ions formed at different temperatures.

Temperature (°C)	$K_w = 10^{14}$	$\log K_w$
20	0.68	14.17
25	1.01	14.0
30	1.47	13.83
33	2.09	13.68

$K_w = [\text{H}^+] + [\text{OH}^-]$; $\text{pH} = -\log [\text{H}^+]$; $[\text{H}^+] = 10^{-\text{pH}}$; $\text{pOH} = -\log [\text{OH}^-]$; $[\text{OH}^-] = 10^{-\text{pOH}}$. $\log K_w = \text{pH} + \text{pOH}$, and $[\text{OH}^-] = 10^{(\text{pH} - \log K_w)}$.

Phenolphthalein has a pH range of 8.0 to 9.6, which is a suitable indicator for the first endpoint, while methyl orange has a pH range of 3.1 to 4.4, which is suitable for the second endpoint. Therefore, mixtures of carbonate and bicarbonate or carbonate and hydroxide can be titrated with standard HCl to both endpoints. Table 4 depicts the correlation between titration volume and carbonate titrations.

Table 4. Relationship of titration volume in carbonate titrations.

Substance	Relationship for Qualitative Identification	Millimol Substance
NaOH	$v_2 = 0$	$M \times v_1$
Na_2CO_3	$V_1 = v_2$	$M \times v_1$
$\text{NaOH} + \text{Na}_2\text{CO}_3$	$V_1 > v_2$	NaOH: $M(v_1 - v_2)$ Na_2CO_3 : $M \times v_2$
$\text{NaHCO}_3 + \text{Na}_2\text{CO}_3$	$V_1 < v_2$	NaHCO_3 : $M(v_2 - v_1)$ Na_2CO_3 : $M \times v_1$

2.2.4. Experimental Design

Statistical design of experiments (DOE) is an effective method for devising experiments that, after data analysis, yield valid and objective conclusions. Two main applications of experimental setup were evaluated to identify the variables that affect the experiment and its optimum conditions [51]. The regression and graphical analysis of the data were performed using Design Expert 13.0.11.0 (Stat-Ease Inc., Minneapolis, MN, USA). The Box–Behnken design (BBD) is the most common RSM design. To obtain optimal levels of CO_2 gas absorption and mass transfer coefficient, RSM was used to analyze the response patterns and determine the optimal combination of variables expected to produce optimal conditions. This study involved three variables labeled X_1 (absorption time), X_2 (absorption flow rate of 0.1 M NaOH), and X_3 (absorption concentration) (CO_2 gas flow rate). This experiment's experimental design is outlined in Table 1. CO_2 is the absorption flow rate, and CO_2 is the gas mass transfer coefficient, denoted by Y_1 and Y_2 , respectively. The relationship between classified and actual variables is expressed as Equation (10) for statistical analysis.

$$x_i = \left(\frac{X_1 - X_2}{\Delta X} \right) \quad (10)$$

where, x_i represents the independent variable or its dimensionless value, X_1 is the independent real value, X_2 is the independent real value at the center point, and ΔX is the step change value. The elimination of lead is the dependent variable or the response. In

addition, the behavior of the system is described by the following second-order polynomial model, Equation (11).

$$Y = \beta_0 + \sum_{i=1}^k \beta_i x_i + \sum_{i=1}^k \beta_{ii} x_i^2 + \sum_{i=1}^k \sum_{j=1}^k \beta_{ij} x_i x_j + \epsilon \quad (11)$$

where, Y is the predicted response; x_i, x_j, \dots, x_k are the input variables affecting the Response Y ; $x_i^2, x_j^2, \dots, x_k^2$ are the square effects; $x_i x_j, x_i x_k$, and $x_j x_k$ are the interaction effects; β_0 is the intercept term; β_i ($i = 1, 2, \dots, k$) is the linear effect; β_{ii} ($i = 1, 2, \dots, k$) is the square effect; β_{ij} ($i = 1, 2, \dots, k; j = 1, 2, \dots, k$) is the interaction effect; and ϵ is random error. For this research, Equation (11) is written as Equation (12).

$$Y_i = \beta_0 + \beta_1 x_1 + \beta_2 x_2 + \beta_3 x_3 + \beta_{11} x_{21} + \beta_{22} x_{22} + \beta_{33} x_{23} + \beta_{12} x_1 x_2 + \beta_{13} x_1 x_3 + \beta_{23} x_2 x_3 \quad (12)$$

The data from Table 5 were used for the ANOVA and multiple regression analyses in the Box–Behnken design with polynomial model Equation (12).

Table 5. Design and analysis of experiments for absorption.

Run	Factor 1 A: X_1 min	Factor 2 B: X_2 L/min	Factor 3 C: X_3 L/min	Response 1 Y_1 L/min	Response 2 Y_2 mol/min m ² atm
1	10	2	3	1.574	1.2882
2	45	3.5	3	2.9651	1.3965
3	45	3.5	3	2.9651	1.3965
4	80	3.5	2	1.9716	1.2965
5	45	2	5	3.9418	1.399
6	80	2	3	2.5611	1.3483
7	45	5	2	1.9756	1.2813
8	45	3.5	3	2.9651	1.3965
9	10	3.5	5	2.9438	1.299
10	45	3.5	3	2.9611	1.3565
11	45	2	2	1.756	1.251
12	45	5	5	3.9418	1.4102
13	80	5	3	2.9611	1.3883
14	45	3.5	3	2.9671	1.3965
15	10	5	3	1.9692	1.295
16	10	3.5	2	1.7756	1.279
17	80	3.5	5	3.9438	1.4365

Information: A: X_1 —absorption time, B: X_2 —absorbent flow rate, C: X_3 —CO₂ flow rate, Y_1 —CO₂ absorption rate (L/min), and Y_2 —CO₂ gas mass coefficient (mol/min. m² atm).

From the data in Table 5, it can be seen that there is an increase in CO₂ absorption rate and CO₂ gas mass transfer coefficient with absorption time and CO₂ gas flow rate. Table 6 displays BBD and the response of various parameters to distinct absorption conditions.

Table 6. BBD and the response of different parameters at various absorption conditions.

Run	F ₁ A: X_1 (Absorption Time), min	F ₂ B: X_2 (pH)	R ₁ [OH] [−] mol/L	R ₂ CO ₃ ^{2−} mol/L	R ₃ HCO ₃ [−] mol/L	R ₄ 2HCO ₃ [−] mol/L	R ₅ CO ₃ ^{2−} mol/L	R ₆ HCO ₃ [−] mol/L	R ₇ Number of Moles of CO ₂ mol/L	R ₈ The Total Volume of CO ₂ Absorbed L
1	0	13.217	243.781	27.8	0	244.64	0.859	0	0.859	0.7216
2	10	12.957	134	20.6	27.4	181.28	47.28	12.56	47.28	39.72
3	20	12.377	35.24	15.8	27.5	139.04	103.803	0	102.963	86.566
4	30	10.867	1.089	12.8	27.4	112.64	111.551	16.929	128.48	108.02
5	40	10.367	0.329	10.7	27.3	92.4	92.071	55.769	147.84	124.297
6	50	10.057	0.1687	8.7	27.3	76.56	76.3913	87.289	162.68	137.614
7	60	9.827	0.0993	7.1	27.8	62.48	62.381	119.779	182.16	153.15
8	60	9.827	0.0993	7.1	27.8	62.48	62.381	119.779	182.16	153.15
9	30	10.867	1.089	12.8	27.4	112.64	111.551	16.929	128.48	108.02
10	20	12.377	35.24	15.8	27.5	139.04	103.803	0	102.963	86.566
11	30	10.867	1.089	12.8	27.4	112.64	111.551	55.769	147.84	124.297
12	30	10.867	1.089	12.8	27.4	112.64	111.551	55.769	147.84	124.297
13	0	13.217	243.781	27.8	0	244.64	0.859	0	0.859	0.7216

3. Results and Discussion

3.1. ANOVA in the Regression Model

The data in Table 5 was taken into account for ANOVA and multiple regression analyses in the Box–Behnken design using polynomial model Equation (12). The results are shown in Tables 7 and 8.

Table 7. Analysis of variance of CO₂ gas absorption flow rate (Y₁, Fa).

Source	Sum of Squares	df	Mean Square	F-Value	p-Value	Effect
Model	9.44	9	1.05	25.44	0.0002	s
A-X ₁	1.04	1	1.04	25.27	0.0015	s
B-X ₂	0.1475	1	0.1475	13.58	0.0506	s
C-X ₃	3.13	1	3.13	75.99	<0.0001	s
AB	5.76×10^{-6}	1	5.76×10^{-6}	0.0001	0.9909	ns
AC	0.1074	1	0.1074	2.61	0.1505	ns
BC	0.0236	1	0.0236	0.5719	0.4742	ns
A ²	0.9369	1	0.9369	22.72	0.0020	s
B ²	0.2162	1	0.2162	5.24	0.0558	ns
C ²	0.0759	1	0.0759	1.84	0.2170	ns
Residual	0.2886	7	0.0412	-	-	-

Information: A: X₁—absorption time, B: X₂—absorbent flow rate, C: X₃—CO₂ gas flow rate, s—significant, ns—not significant.

Table 8. Analysis of variance of CO₂ gas mass transfer coefficient.

Source	Sum of Squares	df	Mean Square	F-Value	p-Value	Effect
Model	0.0523	9	0.0058	12.86	0.0014	s
A-X ₁	0.0087	1	0.0087	19.22	0.0032	s
B-X ₂	0.0011	1	0.0011	20.35	0.0500	s
C-X ₃	0.0241	1	0.0241	53.31	0.0002	s
AB	0.0003	1	0.0003	0.6098	0.4604	ns
AC	0.0034	1	0.0034	7.58	0.0284	s
BC	0.0001	1	0.0001	0.2093	0.6612	ns
A ²	0.0046	1	0.0046	10.20	0.0152	s
B ²	0.0027	1	0.0027	6.04	0.0436	s
C ²	0.0084	1	0.0084	18.52	0.0036	s
Residual	0.0032	7	0.0005	-	-	-

Information: A: X₁—absorption time, B: X₂—absorbent flow rate, C: X₃—CO₂ gas flow rate, s—significant, ns—not significant.

Table 7 shows the report contains a summary of the criteria and constraints used to generate the optimal solution for the process; all the criteria were applied to find the optimal setting. A solution is a search of all the solutions given to see which one best meets the specified criteria. The CO₂ absorption design and optimization model in this study is suitable for use as an alternative in the chemical industry or industries that emit a lot of CO₂ gas into the air, such as the cement industry, exhaust gas sources, natural gas burners, natural gas turbines, fuel-fired power plants, and coal, to absorb CO₂ gas before it is discharged into the air by adjusting the amount as needed. For example, the CO₂ gas produced is adjusted to the CO₂ absorption capacity and the scale ratio according to the needs of the desired CO₂ absorption capacity. The research model can be used as a pilot plant for CO₂ absorption before being discharged into the air as an alternative in the future to reduce CO₂ emissions into the air, which can cause global warming [28–40].

3.2. Fitting the Model

Analysis of variance (ANOVA) and multiple regression analysis were employed to evaluate the effects of individual and interaction factors using Design Expert 13. Box–Behnken design is the most frequently used RSM design, and the model equation is applied

to predict the optimum CO₂ gas absorption flow rate (Y_1) and CO₂ gas mass transfer coefficient (Y_2).

The final equation in terms of coded factors is presented in Equation (13):

$$Y_1 = 2.96 + 0.37 X_1 + 0.14 X_2 + 1.35 X_3 + 0.0012 X_1 X_2 + 0.213 X_1 X_3 - 0.1 X_2 X_3 - 0.47 X_1^2 - 0.23 X_2^2 - 0.28 X_3^2 \quad (13)$$

The final equation in terms of actual factors is presented in Equation (14):

$$Y_1 = -2.44 + 0.036 X_1 + 0.897 X_2 + 1.07 X_3 + 0.000023 X_1 X_2 + 0.00304 X_1 X_3 - 0.033 X_2 X_3 - 0.00039 X_1^2 - 0.1007 X_2^2 - 0.07 X_3^2 \quad (14)$$

The model equation was applied to predict the optimum CO₂ gas mass transfer coefficient (Y_2 , k_{og}).

The final equation in terms of coded factors is shown in Equation (15):

$$Y_2 = 1.39 + 0.034 X_1 + 0.012 X_2 + 0.119 X_3 + 0.0083 X_1 X_2 + 0.038 X_1 X_3 - 0.0063 X_2 X_3 - 0.033 X_1^2 - 0.026 X_2^2 - 0.092 X_3^2 \quad (15)$$

The final equation in terms of actual factors is shown in Equation (16):

$$Y_2 = 0.82 + 0.00122 X_1 + 0.0863 X_2 + 0.18 X_3 + 0.00016 X_1 X_2 + 0.00543 X_1 X_3 - 0.0021 X_2 X_3 - 0.00003 X_1^2 - 0.01132 X_2^2 - 0.023 X_3^2 \quad (16)$$

where Y_1 is the predicted CO₂ gas absorption flow rate response, and Y_2 is the CO₂ gas mass transfer coefficient. Meanwhile, X_1 , X_2 , and X_3 are independent variables for absorption time, absorption flow rate, and CO₂ gas flow rate, respectively.

Based on the equation, it was shown that the influence of absorption times (X_1), absorption flow rate (X_2), and CO₂ gas flow rate affected the CO₂ absorption rate and CO₂ gas mass transfer coefficient. These effects can be observed from the intercept and coefficients of the three optimization equations.

Figure 2 illustrates the influence of interactive variables. Figure 2a displays the experimental and predicted data plot. The value predicted by the design response surface equation has a high degree of accuracy ($R^2 = 0.97$) and has an intercept of 1.00663. The distribution point spread above the prediction line demonstrates this. To obtain a respectable model, we must examine the normal probability value (%). As shown in Figure 2b, the proposed equation model is appropriate for predicting the CO₂ gas absorption flow rate (Y_1) and CO₂ gas mass transfer coefficient (Y_2) when using absorbent NaOH 0.1 M. The value predicted by the design response surface equation is precise ($R^2 = 0.94$) and has an intercept of 1.25048. The correlation of the variable effects on variable responses can be seen in Figures 2–6.

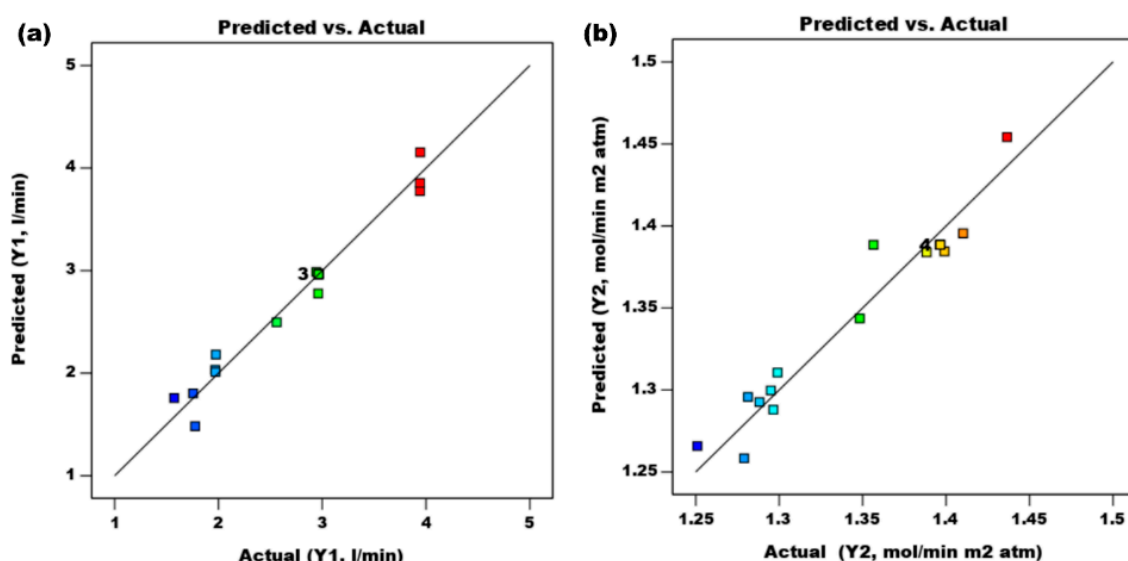


Figure 2. Correlation between actual and predicted results for CO₂ gas mass flow rate and CO₂ gas mass damping coefficient: (a) $R^2 = 0.97$ and (b) $R^2 = 0.94$.

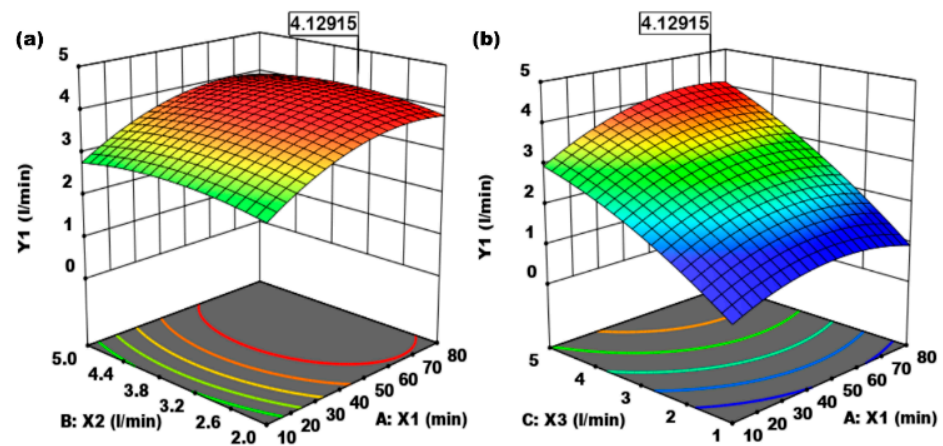


Figure 3. (a) Effect of absorption time (X_1 , min) and absorbent flow rate (X_2 , L/min) on CO₂ gas absorption flow rate (Y_1 , L/min). (b) Effect of absorption time (X_1 , min) and CO₂ gas flow rate (X_3 , L/min) on CO₂ gas absorption flow rate (Y_1 , L/min).

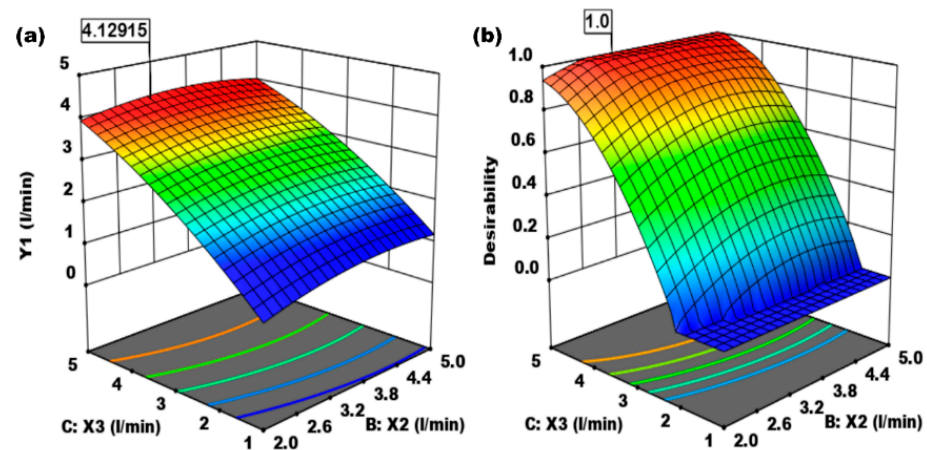


Figure 4. (a) Effect of absorbent flow rate (X_2 , L/min) and CO₂ gas flow rate (X_3 , L/min) on CO₂ absorption flow rate. (b) Effect of absorbent flow rate (X_2 , L/min) and CO₂ gas flow rate (X_3 , L/min) on the desirability.

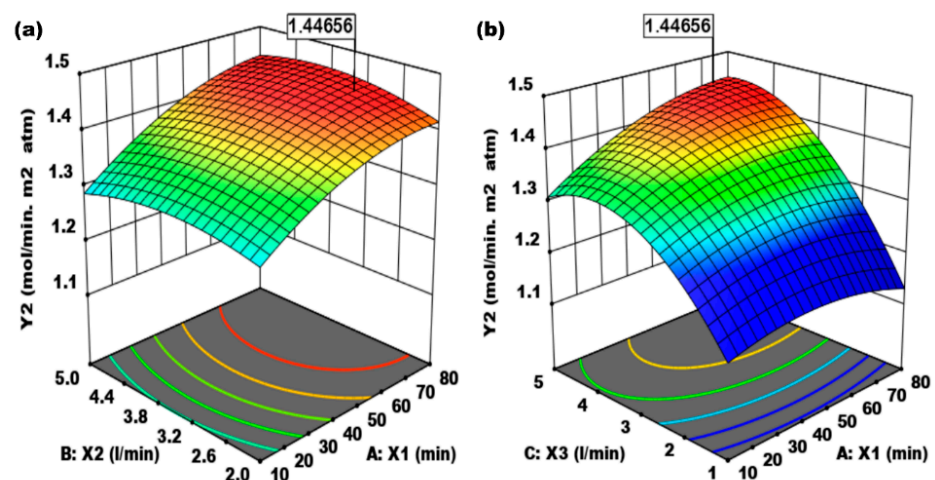


Figure 5. (a) Effect of absorption time (X_1 , min) and absorbent flow rate (X_2 , L/min) on mass transfer coefficient of CO₂ gas (mol/min m² atm). (b) Effect of absorption time (X_1 , min) and CO₂ gas flow rate (X_3 , L/min) on mass transfer coefficient of CO₂ gas (mol/min m² atm).

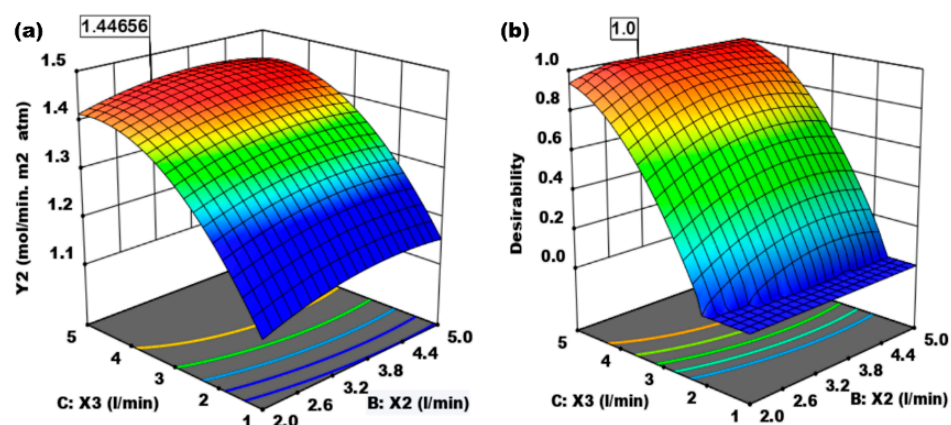
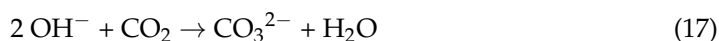


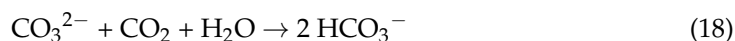
Figure 6. (a) Effect of the absorbent flow rate of 0.1 M NaOH (X_2 , L/min) and CO_2 gas flow rate (X_3 , L/min) on mass transfer coefficient of CO_2 gas. (b) Effect of the absorbent flow rate (X_2 , L/min) and CO_2 flow rate (X_3 , L/min) on the desirability.

In Figure 2, NaOH is wholly neutralized at the phenolphthalein endpoint, Na_2CO_3 is half neutralized, and HCO_3^- has not responded. From the phenolphthalein endpoint to the methyl symbol endpoint, the bicarbonate is neutralized. Therefore, only a few drops of titrant will be required for the NaOH to change from pH 8 to 4, which will be corrected with a blank indicator. As shown in Table 4, v_1 is the volume of acid in millimeters used from the start of the titration to the phenolphthalein endpoint, and v_2 is the volume from the phenolphthalein endpoint to methyl orange.

During the absorption of CO_2 gas, a reaction occurs between CO_2 and OH^- because the pH value decreases, and the reaction proceeds according to the following criteria. If pH = 11.5, the reaction is:



If pH = 10, the reaction is:



If pH = 11, the reaction is:



After absorption of CO_2 gas, a mixture of OH^- , CO_3^{2-} , and HCO_3^- ions occurs in the solution [25,34]. Sample titration using HCl whose molarity is known (HCl standard) will obtain two equivalence points. In the first step, OH^- reacts as a whole, whereas HCO_3^- reacts only in the second step, and CO_3^{2-} splits in both. Therefore, direct calculation of the concentration is not possible but can be calculated if the p -value and m -value have been determined. The p -value (phenolphthalein price) is the volume of titration used to titrate 1 mol/L HCl for 1000 mL so that the color of the phenolphthalein indicator changes (or to a pH of 8.2 using a glass electrode). The M -value (methyl orange value) is the volume used to titrate 1000 mL of HCl mol/L (1 M) sample until the color of the methyl orange indicator changes (or at pH 4.3 by using a glass electrode). The formulas used in this regard are as follows: $p\text{-value} = V \times M \times 1000/\text{aliquot}$, where V = volume of titration (mL), M = molarity of HCl used, aliquots = volume of sample titrated, $C[\text{OH}^-] = 10^{(\text{pH}-13.83)}$, $C[\text{CO}_3^{2-}] = P\text{-value} - C[\text{OH}^-]$, and $C[\text{HCO}_3^-] = M\text{-value} - 2 \times P\text{-value} + C[\text{OH}^-]$.

CO_2 absorption is a function of pH; the reaction that occurs is a function of pH; the increasing absorption of CO_2 , which continues to increase, is a function of pH, sol-

ubility, thermal, and longitudinal diffusion; the mechanism of mass contraction is the driving force in the form of differences in CO₂ concentrations and the partial pressure of each component and total pressure; the formula used is pH dependent, as it is determined by pH [51,52], and the reaction is according to the following criteria. If the pH value < 4.5, then $C[\text{CO}_3^{2-}] = P - \text{value} - C[\text{H}^+]$. If the pH value is between 4.5–8.3, then $C[\text{HCO}_3^-] = P - \text{value}$. If the pH value is between 8.3–9.5, then $C[\text{HCO}_3^-] = M - \text{value} - 2 \times P - \text{value}$. Suppose the pH value is >9.5. Then $C[\text{HCO}_3^-]$ is calculated from Equation (2).

Figure 3a,b shows the 3-D optimization of the effect of absorption time (minutes), the flow rate of 0.1 M NaOH absorbent (L/min), and the flow rate of CO₂ gas mixed with air (L/min) on the absorption rate of CO₂ gas in the Raschig packing tower ring.

Figure 3a shows the effect of absorption time (X_1 , min) and absorbent flow rate (X_2 , L/min) on CO₂ gas absorption flow rate (Y_1 , L/min). The effect of the two independent variables on the response variable (CO₂ gas absorption) increased, and optimal conditions were reached at 4.13 L/min. Figure 3b shows the desired optimization of the effect of absorption time (minutes), the flow rate of 0.1 M NaOH absorbent (L/min), and air-mixed CO₂ flow rate (L/min) on the absorption rate of CO₂ gas in the Raschig ring packing tower. The effects of absorption time (X_1 , min) and CO₂ gas flow rate (X_2 , L/min) on CO₂ gas absorption rate (Y_1 , L/min) increased until it reached the optimum condition of 4.13 (L/min).

Figure 4a,b show the 3-D optimization of the effect of absorption time (minutes), the flow rate of 0.1 M NaOH absorbent (L/min), and CO₂ gas flow rate (L/min) on the mass transfer coefficient of CO₂ gas in the Raschig ring packing tower. Figure 4a shows the effect of absorbent flow rate (X_2 , L/min) and CO₂ gas flow rate (X_3 , L/min) on the CO₂ absorption flow rate. The absorption rate of CO₂ gas increases until it reaches optimum conditions, which are reached at a value of 4.1292. Figure 4b shows the effect of absorbent flow rate (X_2 , L/min) and CO₂ gas flow rate (X_3 , L/min) on desirability. Desirability can be increased by choosing the proper criteria in planning the constraints to achieve the best optimal conditions. The best condition is achieved at the desired value of 0.99999.

Figure 5a shows the effect of absorbent flow rate (X_2 , L/min) and CO₂ gas flow rate (X_3 , L/min) on the CO₂ absorption flow rate. The CO₂ absorption flow rate continues to increase so that optimum conditions are reached at 4.13 L/min. Figure 5b shows the desired optimization of the effects of absorption time (minutes), the flow rate of 0.1 M NaOH absorbent (L/min), and the CO₂ gas flow rate (L/min) on the mass transfer coefficient of CO₂ gas in the tower packing Raschig ring. Based on the analysis and optimization of 3-D plots, the optimum conditions for the CO₂ uptake rate are 1.44656 L/min, and the mass transfer coefficient for CO₂ gas is 1.44656 mol/min m² atm.

Figure 6a shows the effect of the absorbent flow rate of 0.1 M NaOH (X_2 , L/min) and CO₂ gas flow rate (X_3 , L/min) on the mass transfer coefficient of CO₂ gas. The greater the flow rate of the absorbent and the flow rate of CO₂ gas, the higher the mass damping value, and the faster the mass locking occurs due to the driving force difference in CO₂ gas concentration in the absorbent and air. Optimal mass absorption conditions are achieved at 1.44656 mol/min m² or mol/min m² atm. Figure 6b is the effect of 0.1 M NaOH absorbent flow rate (X_2 , L/min) and CO₂ flow rate (X_2 , L/min) on optimal desirability based on a design to determine constraints that produce the best-desired desire. The optimum desirability value is 0.9999 (≈1). Numerical optimization and desirability ramps are shown in Figures 7 and 8, respectively.

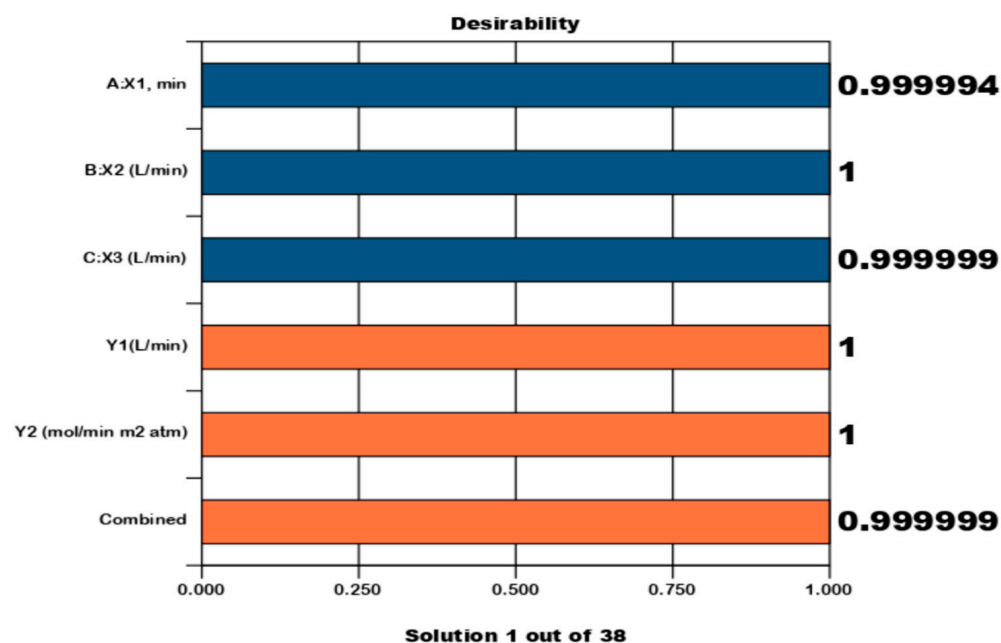


Figure 7. Numerical optimization bar graph (Pareto graph), The bar graph is a graphical view of each optimal solution. The optimal factor settings are shown: absorption time (X_1), absorbent flow rate (X_2), CO_2 flow rate (X_3), CO_2 absorption rate (Y_1), and CO_2 gas mass coefficient (Y_2).

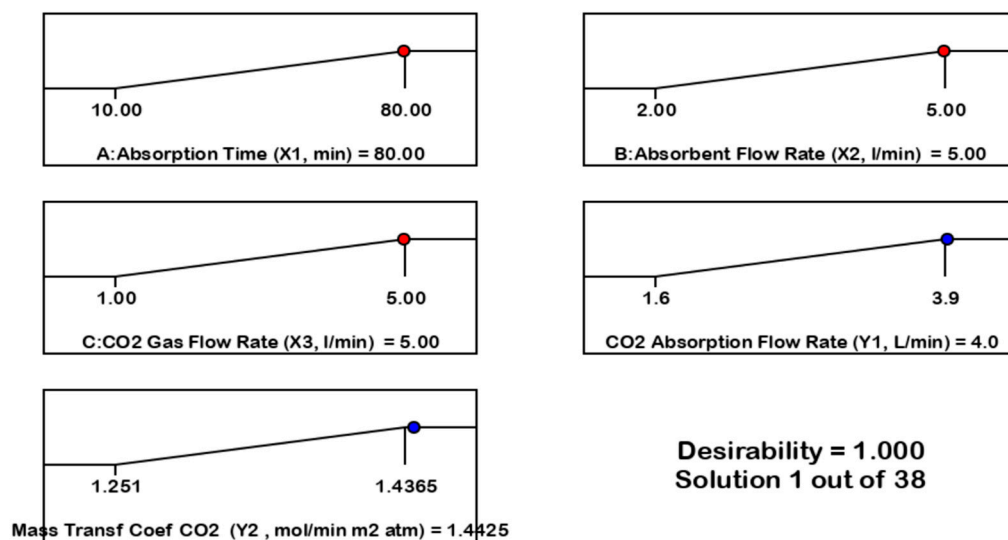


Figure 8. Desirability ramp for numerical optimization of three goals, i.e., the absorption time (X_1 , min), absorbent flow rate (X_2 , L/min), CO_2 gas flow rate (X_3 , L/min), on CO_2 absorption flow rate (Y_1 , L/min), and mass transfer coefficient (Y_2 , mol/min m² atm) as the response variable.

Figure 9 shows the 3-D optimization of the effect of absorption time (min) and pH on the formation of HCO_3^- and CO_3^{2-} as a result of the reactions between $2\text{OH}^- + \text{CO}_2$ and $\text{CO}_3^{2-} + \text{CO}_2 + \text{H}_2\text{O}_2 + \text{HCO}_3^-$, conditions under which the optimum was achieved at 154.994 mol/L HCO_3^- and 105.664 mol/L CO_3^{2-} . This shows that absorption also occurs chemically, according to pH. This reaction occurs at a pH of 9.5–11, forming CO_3^{2-} and HCO_3^{2-} due to the reaction of OH^- and CO_2 , whose products can be used to meet the needs of cosmetics and food ingredients.

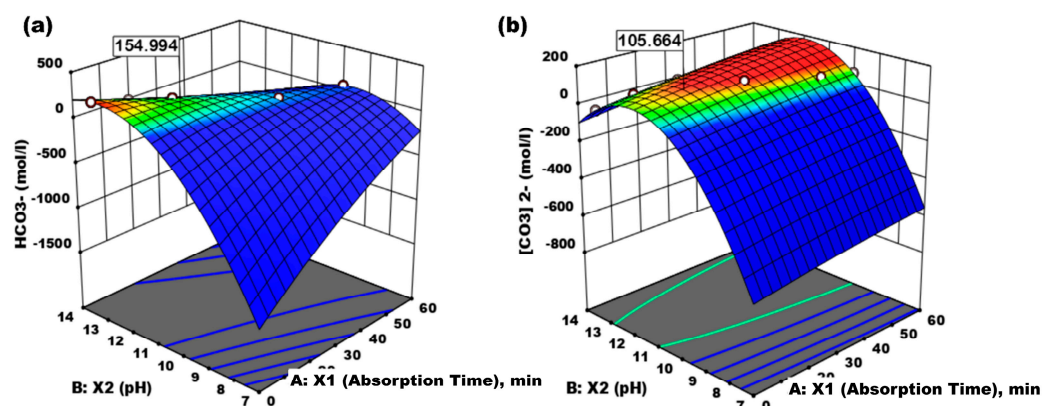


Figure 9. (a) Effect of absorption time (X_1 , min) and absorbent pH (X_2) on HCO_3^- formed. (b) Effect of absorption time (X_1 , min) and absorbent pH (X_2) on CO_3^{2-} formed.

Figure 10 shows the numerical optimization bar graph (Pareto graph) for desirability. The bar graph is a graphic display for each optimal solution. Optimal factor settings are shown with red bars, and optimal response predicted values are shown in blue. Optimum conditions for the desirability of each factor are, respectively, absorption time (X_1 , min), absorbent flow rate (X_2 , L/min), and CO_2 gas flow rate mixed with air = 0.99, CO_2 absorption desire rate (Y_1 , L/min), and mass transfer coefficient CO_2 gas (Y_2 , mol/min m^2 atm) = 0.999 each; and combined desire = 0.99.

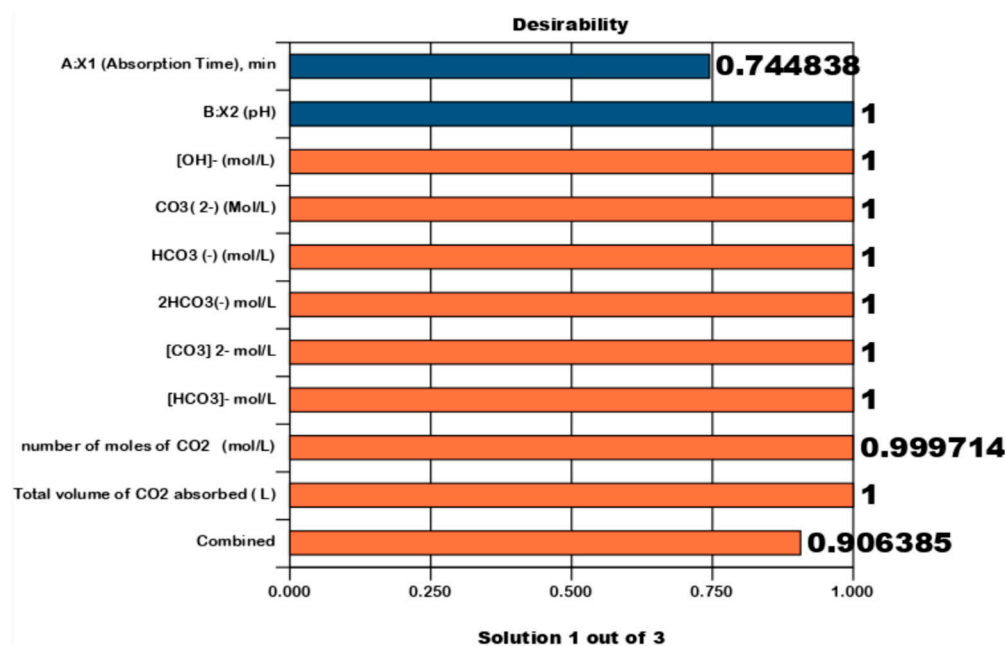


Figure 10. Numerical optimization bar graph (Pareto graph). The bar graph is a graphical view of each optimal solution. Optimal factors settings are shown: absorption time (X_1), pH (X_2), OH^- (mol/L), CO_3^{2-} (mol/L), HCO_3^{2-} (mol/L), 2HCO_3^{2-} (mol/L), CO_3^{2-} (mo/L), HCO_3^{2-} (mol/L), number of moles of CO_2 (mol/L), and total volume of CO_2 absorbed (L).

Figure 11 is the desirability ramp for numerical optimization of the 3-D optimization of the effect of absorption time (minutes) and pH on the formation of HCO_3^- and CO_3^{2-} as a result of the reaction between $2\text{OH}^- + \text{CO}_2 \rightarrow \text{CO}_3^{2-} + \text{H}_2\text{O}$ and $\text{CO}_3^{2-} + \text{CO}_2 + \text{H}_2\text{O} \rightarrow 2\text{HCO}_3^-$, optimal conditions achieved, i.e., absorption time = 15.3097 (X_1 , min), pH = 11.52 (X_2), CO_3^{2-} = 105.664 mol/L, HCO_3^{2-} = 154.994 mol/L, a total of CO_2 = 76.9359 L, and desirability = 0.91.

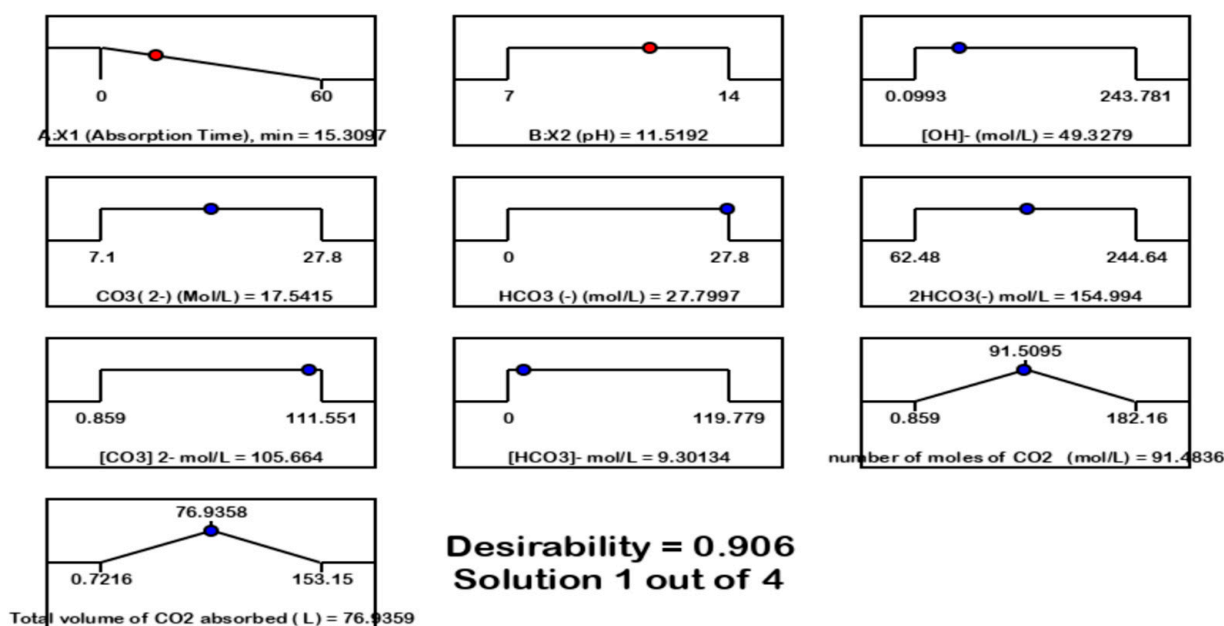


Figure 11. Desirability ramp for numerical optimization of the 3-D optimization of the effect of absorption time (minutes) and pH on the formation of HCO₃⁻ and CO₃²⁻ as a result of the reaction between 2OH⁻ + CO₂, desirability = 0.906.

Table 9 illustrates the numerical optimization. Constraints are designed according to appropriate criteria to produce reliable validity and high accuracy by looking at the influence and correlation between each independent variable and the response variable to produce the correct constraints and high desirability.

$$D = (d_1^{r_1} \cdot d_1^{r_2} \dots d_1^{r_n})^{\frac{1}{\sum r_i}} = \left(\prod_{i=1}^n d_i^{r_i} \right)^{\frac{1}{\sum r_i}} \quad (20)$$

where, n is the number of responses in the measure; if all the important values are the same, the simultaneous objective function reduces to the normal form for desirability.

Table 9. Numerical optimization constraints.

Name	Goal	Lower Limit	Upper Limit	Lower Weight	Upper Weight	Importance
A:X ₁ , min	maximize	10	80	1	1	3
B:X ₂ (L/min)	maximize	2	5	1	1	3
C:X ₃ (L/min)	maximize	1	5	1	1	3
Y ₁ (L/min)	maximize	1.574	3.9438	1	1	3
Y ₂ (mol/min m ² atm)	maximize	1.251	1.4365	1	1	3

Information: X₁—Absorption Time, X₂—Absorbent flow rate, X₃—CO₂ gas flow rate, Y₁—Absorption flow rate, Y₂—Mass transfer coefficient.

For the goal of maximum, the desirability will be defined by the following formulas:

$$d_i = \begin{cases} 0, & Y_i \leq \text{Low}_i \\ \left[\frac{Y_i - \text{Low}_i}{\text{High}_i - \text{Low}_i} \right]^{wt_i}, & \text{Low}_i < Y_i < \text{High}_i \\ 1, & Y_i \geq \text{High}_i \end{cases} \quad (21)$$

For absorption time criteria, X₁ (10–80 min) maximum goals: optimum X₁ = 80 min absorption flow rate; X₂ (2–5 L/min) maximum goals: optimum X₂ = 5 L/min, CO₂ gas

flow rate, X_3 (2–5 L/min): optimum $X_3 = 5$ L/min on absorption flow rate $Y_1 = 3.967$ L/min and desirability = 0.999999 ≈ 1 . Desirability ramp for numerical optimization of three goals, i.e., the absorption time, X_1 (10–80 min), absorbent flow rate, X_2 (2–5 L/min) CO_2 gas flow rate, X_3 (2–5 L/min), on mass transfer coefficient (Y_2 , mol/min m^2 atm) as the response variable. Optimum condition: $X_1 = 5$ L/min, $X_2 = 5$ L/min, $X_3 = 5$ L/min, $Y_2 = 1.442$ mol/min m^2 atm and desirability = 0.999999 ≈ 1 .

Table 10 presents desirability function optimization. Analysis of variance (ANOVA) for responses to CO_2 gas absorption flow rate (Y_1) indicates that effects of individual factors (absorption time, absorption flow rate, and CO_2 gas flow rate) are significant for degree of confidence $\geq 95\%$ ($p\text{-value} \leq 0.05$). The RSM model selected is a quadratic model, $R^2 = 0.97$, $CV = 7.4$, and the model is very significant.

Table 10. Optimization using the desirability function.

Number	X_1 , min	X_2 (L/min)	X_3 (L/min)	Y_1 (L/min)	Y_2 (mol/min m^2 atm)	Desirability	
1	80.000	5.000	5.000	3.967	1.442	1.000	Selected
2	79.999	5.000	5.000	3.967	1.442	1.000	
3	80.000	5.000	4.984	3.960	1.443	0.999	
4	79.999	4.988	4.999	3.970	1.443	0.999	
5	79.668	5.000	5.000	3.971	1.442	0.999	
6	80.000	5.000	4.967	3.952	1.443	0.998	
7	79.372	5.000	5.000	3.974	1.442	0.998	
8	79.999	5.000	4.961	3.950	1.443	0.998	
9	80.000	4.970	5.000	3.976	1.443	0.998	
10	79.015	5.000	5.000	3.977	1.442	0.997	
11	80.000	4.945	5.000	3.982	1.444	0.996	
12	80.000	4.933	5.000	3.985	1.444	0.996	
13	80.000	5.000	4.920	3.930	1.444	0.995	
14	80.000	4.912	5.000	3.991	1.445	0.994	
15	77.458	5.000	5.000	3.991	1.441	0.993	

Information: X_1 —Absorption time, X_2 —Absorbent flow rate, X_3 — CO_2 gas flow rate, Y_1 —Absorption flow rate, Y_2 —Mass transfer coefficient.

Analysis of variance (ANOVA) for the response variable CO_2 gas mass transfer coefficient (Y_2) showed the influence of individual factors and significant interaction for the degree of confidence $\geq 95\%$ ($p\text{-value} \leq 0.05$), except for the interaction effect of $X_1 X_2$ and $X_2 X_3$, which was not significant. Therefore, the RSM model was chosen as a quadratic model with $R^2 = 0.94$ and $CV = 4$, and the model is significant.

4. Conclusions

This study investigated CO_2 gas absorption with NaOH absorbent continuous system in Raschig ring packing column using Box–Behnken design. Based on the results and discussion, the optimization conditions assumed a maximum point for desirability. Experiments were performed based on absorption time, the absorption flow rate of 0.1 M NaOH, and the CO_2 gas flow rate. The results showed that the absorption of CO_2 gas in the air was optimized by using 0.1 M NaOH absorbent in the tower of the Raschig ring stuffing material using the response surface methodology (RSM), with an absorption rate of 4 L/min, a mass transfer coefficient of 1.4425 mol/min m^2 atm, and desirability 0.999 ≈ 1 .

Author Contributions: Conceptualization, methodology, investigation, writing—original draft, J.; conceptualization, writing—review and editing, and validation, H.H.; writing—review and editing, M.Z. (Muhammad Zaki), L.M. and M.Z. (Mirna Zulrika); formal analysis and writing—review and editing, F.N. and A. All authors have read and agreed to the published version of the manuscript.

Funding: This research received no external funding.

Institutional Review Board Statement: Not applicable.

Informed Consent Statement: Not applicable.

Data Availability Statement: Not applicable.

Acknowledgments: The authors are grateful to the Chemical Engineering Department, Faculty of Engineering at Universitas Syiah Kuala, for technical support.

Conflicts of Interest: The authors declare that there are no conflict of financial or non-financial interest.

References

- Hu, Y.; Li, R.; Du, L.; Ren, S.; Chevallier, J. Could SO₂ and CO₂ Emissions Trading Schemes Achieve Co-Benefits of Emissions Reduction? *Energy Policy* **2022**, *170*, 113252. [\[CrossRef\]](#)
- De Troeyer, K.; De Man, J.; Vandebroek, E.; Vanoirbeek, J.A.; Hoet, P.H.; Nemery, B.; Vanroelen, C.; Casas, L.; Ronsmans, S. Identifying Cleaning Products Associated with Short-Term Work-Related Respiratory Symptoms: A Workforce-Based Study in Domestic Cleaners. *Environ. Int.* **2022**, *162*, 107170. [\[CrossRef\]](#) [\[PubMed\]](#)
- Wang, C.; Zhang, J.L.; Gao, X.H.; Zhao, T.S. Research Progress on Iron-Based Catalysts for CO₂ Hydrogenation to Long-Chain Linear α -Olefins. *J. Fuel Chem. Technol.* **2023**, *51*, 67–85. [\[CrossRef\]](#)
- Zou, C.; Xiong, B.; Xue, H.; Zheng, D.; Ge, Z.; Wang, Y.; Jiang, L.; Pan, S.; Wu, S. The Role of New Energy in Carbon Neutral. *Pet. Explor. Dev.* **2021**, *48*, 480–491. [\[CrossRef\]](#)
- Fang, K.; Li, C.; Tang, Y.; He, J.; Song, J. China's Pathways to Peak Carbon Emissions: New Insights from Various Industrial Sectors. *Appl. Energy* **2022**, *306*, 118039. [\[CrossRef\]](#)
- Madejski, P.; Chmiel, K.; Subramanian, N.; Kuś, T. Methods and Techniques for CO₂ Capture: Review of Potential Solutions and Applications in Modern Energy Technologies. *Energies* **2022**, *15*, 887. [\[CrossRef\]](#)
- Lang, X.D.; He, X.; Li, Z.M.; He, L.N. New Routes for CO₂ Activation and Subsequent Conversion. *Curr. Opin. Green Sustain. Chem.* **2017**, *7*, 31–38. [\[CrossRef\]](#)
- Aghel, B.; Janati, S.; Alobaid, F.; Almoslh, A.; Epple, B. Application of Nanofluids in CO₂ Absorption: A Review. *Appl. Sci.* **2022**, *12*, 3200. [\[CrossRef\]](#)
- Sattthawong, R.; Koizumi, N.; Song, C.; Prasassarakich, P. Bimetallic Fe-Co Catalysts for CO₂ Hydrogenation to Higher Hydrocarbons. *J. CO₂ Util.* **2013**, *3–4*, 102–106. [\[CrossRef\]](#)
- Xue, L.; Zhang, C.; Wu, J.; Fan, Q.Y.; Liu, Y.; Wu, Y.; Li, J.; Zhang, H.; Liu, F.; Zeng, S. Unveiling the Reaction Pathway on Cu/CeO₂ Catalyst for Electrocatalytic CO₂ Reduction to CH₄. *Appl. Catal. B* **2022**, *304*, 120951. [\[CrossRef\]](#)
- Miao, Z.; Wang, Q.; Zhang, Y.; Meng, L.; Wang, X. In Situ Construction of S-Scheme AgBr/BiOBr Heterojunction with Surface Oxygen Vacancy for Boosting Photocatalytic CO₂ Reduction with H₂O. *Appl. Catal. B* **2022**, *301*, 120802. [\[CrossRef\]](#)
- Guo, L.; Cui, Y.; Li, H.; Fang, Y.; Prasert, R.; Wu, J.; Yang, G.; Yoneyama, Y.; Tsubaki, N. Selective Formation of Linear-Alpha Olefins (LAOs) by CO₂ Hydrogenation over Bimetallic Fe/Co-Y Catalyst. *Catal. Commun.* **2019**, *130*, 105759. [\[CrossRef\]](#)
- Ra, E.C.; Kim, K.Y.; Kim, E.H.; Lee, H.; An, K.; Lee, J.S. Recycling Carbon Dioxide through Catalytic Hydrogenation: Recent Key Developments and Perspectives. *ACS Catal.* **2020**, *10*, 11318–11345. [\[CrossRef\]](#)
- Roy, S.; Cherevotan, A.; Peter, S.C. Thermochemical CO₂ Hydrogenation to Single Carbon Products: Scientific and Technological Challenges. *ACS Energy Lett.* **2018**, *3*, 1938–1966. [\[CrossRef\]](#)
- Ren, S.; Hu, Y.; Zheng, J.; Wang, Y. Emissions Trading and Firm Innovation: Evidence from a Natural Experiment in China. *Technol. Forecast. Soc. Chang.* **2020**, *155*, 119989. [\[CrossRef\]](#)
- Jebabli, I.; Lahiani, A.; Mefteh-Wali, S. Quantile Connectedness between CO₂ Emissions and Economic Growth in G7 Countries. *Resour. Policy* **2023**, *81*, 103348. [\[CrossRef\]](#)
- Xia, C.; Li, Y.; Xu, T.; Chen, Q.; Ye, Y.; Shi, Z.; Liu, J.; Ding, Q.; Li, X. Analyzing Spatial Patterns of Urban Carbon Metabolism and Its Response to Change of Urban Size: A Case of the Yangtze River Delta, China. *Ecol. Indic.* **2019**, *104*, 615–625. [\[CrossRef\]](#)
- Tollefson, J. Trump Pulls United States out of Paris Climate Agreement. *Nature* **2017**, *546*, 22096. [\[CrossRef\]](#)
- Huang, Z.; He, W.; Zhao, L.; Liu, H.; Zhou, X. Processing Technology Optimization for Tofu Curded by Fermented Yellow Whey Using Response Surface Methodology. *Food Sci. Nutr.* **2021**, *9*, 3701–3711. [\[CrossRef\]](#)
- Delanoë, P.; Tchuente, D.; Colin, G. Method and Evaluations of the Effective Gain of Artificial Intelligence Models for Reducing CO₂ Emissions. *J. Environ. Manag.* **2023**, *331*, 117261. [\[CrossRef\]](#)
- Ye, H.; He, X.Y.; Song, Y.; Li, X.; Zhang, G.; Lin, T.; Xiao, L. A Sustainable Urban Form: The Challenges of Compactness from the Viewpoint of Energy Consumption and Carbon Emission. *Energy Build.* **2015**, *93*, 90–98. [\[CrossRef\]](#)
- Malekli, M.; Aslani, A. A Novel Post-Combustion CO₂ Capture Design Integrated with an Organic Rankine Cycle (ORC). *Process Saf. Environ. Prot.* **2022**, *168*, 942–952. [\[CrossRef\]](#)
- Kim, S.; Ko, Y.; Lee, G.J.; Lee, J.W.; Xu, R.; Ahn, H.; Kang, Y.T. Sustainable Energy Harvesting from Post-Combustion CO₂ Capture Using Amine-Functionalized Solvents. *Energy* **2023**, *267*, 126532. [\[CrossRef\]](#)
- Miao, L.; Tang, S.; Li, X.; Yu, D.; Deng, Y.; Hang, T.; Yang, H.; Liang, Y.; Kwan, M.P.; Huang, L. Estimating the CO₂ Emissions of Chinese Cities from 2011 to 2020 Based on SPNN-GNNWR. *Environ. Res.* **2023**, *218*, 115060. [\[CrossRef\]](#)

25. Galán, G.; Martín, M.; Grossmann, I.E. Systematic Comparison of Natural and Engineering Methods of Capturing CO₂ from the Air and Its Utilization. *Sustain. Prod. Consum.* **2023**, *37*, 78–95. [\[CrossRef\]](#)
26. Ibrahim, N.; Cox, S.; Mills, R.; Aftelak, A.; Shah, H. Multi-Objective Decision-Making Methods for Optimising CO₂ Decisions in the Automotive Industry. *J. Clean Prod.* **2021**, *314*, 128037. [\[CrossRef\]](#)
27. Chen, P.; Lu, Y.; Wan, Y.; Zhang, A. Assessing Carbon Dioxide Emissions of High-Speed Rail: The Case of Beijing-Shanghai Corridor. *Transp. Res. D Transp. Environ.* **2021**, *97*, 102949. [\[CrossRef\]](#)
28. Sanjay Kanna Sharma, T.; Jana, J.; Bhamu, K.C.; Song, J.; Sivaselvam, S.; Van Tam, T.; Kang, S.G.; Chung, J.S.; Hur, S.H.; Choi, W.M. Rational Synthesis of Alkaline Earth Metal Vanadates: Structural Origin of MgVO₃ Honeycomb Lattice System and Its Electrochemical Analysis for the Detection of Sulfadiazine. *Chem. Eng. J.* **2023**, *464*, 142673. [\[CrossRef\]](#)
29. Notz, R.; Mangalapally, H.P.; Hasse, H. Post Combustion CO₂ Capture by Reactive Absorption: Pilot Plant Description and Results of Systematic Studies with MEA. *Int. J. Greenh. Gas Control.* **2012**, *6*, 84–112. [\[CrossRef\]](#)
30. Mangalapally, H.P.; Hasse, H. Pilot Plant Study of Post-Combustion Carbon Dioxide Capture by Reactive Absorption: Methodology, Comparison of Different Structured Packings, and Comprehensive Results for Monoethanolamine. *Chem. Eng. Res. Des.* **2011**, *89*, 1216–1228. [\[CrossRef\]](#)
31. Tobiesen, F.A.; Svendsen, H.F.; Juliussen, O. Experimental Validation of a Rigorous Absorber Model for CO₂ Postcombustion Capture. *AIChE J.* **2007**, *53*, 846–864. [\[CrossRef\]](#)
32. Gabrielsen, J. CO₂ Capture from Coal Fired Power Plants. *Bull. Can. Pet. Geol.* **2007**, *55*.
33. Idem, R.; Wilson, M.; Tontiwachwuthikul, P.; Chakma, A.; Veawab, A.; Aroonwilas, A.; Gelowitz, D. Pilot Plant Studies of the CO₂ Capture Performance of Aqueous MEA and Mixed MEA/MDEA Solvents at the University of Regina CO₂ Capture Technology Development Plant and the Boundary Dam CO₂ Capture Demonstration Plant. *Ind. Eng. Chem. Res.* **2006**, *45*, 2414–2420. [\[CrossRef\]](#)
34. Kittel, J.; Idem, R.; Gelowitz, D.; Tontiwachwuthikul, P.; Parrain, G.; Bonneau, A. Corrosion in MEA Units for CO₂ Capture: Pilot Plant Studies. *Energy Procedia* **2009**, *1*, 791–797. [\[CrossRef\]](#)
35. Mejdell, T.; Vassbotn, T.; Juliussen, O.; Tobiesen, A.; Einbu, A.; Knuutila, H.; Hoff, K.A.; Andersson, V.; Svendsen, H.F. Novel Full Height Pilot Plant for Solvent Development and Model Validation. *Energy Procedia* **2011**, *4*, 1753–1760. [\[CrossRef\]](#)
36. Dugas, R.E. *Pilot Plant Study of Carbon Dioxide Capture by Aqueous Mono Ethanol Amin*; University of Texas at Austin: Austin, TX, USA, 2006.
37. Wang, Y.; Chen, H.; Chen, C.; Zhang, Z.; Xu, Y.; Chen, G.; Zhang, Y. Byproducts of the Anammox-Hydroxyapatite Coupling Process—Characterization and Its Adsorption Capacity for Cd(II). *SSRN Electron. J.* **2022**, *49*. [\[CrossRef\]](#)
38. Mimura, T.; Shimojo, S.; Suda, T.; Iijima, M.; Mitsuoka, S. Research and Development on Energy Saving Technology for Flue Gas Carbon Dioxide Recovery and Steam Dioxide Recovery in Power Plant. *Energy Convers. Manag.* **1995**, *36*, 6–9. [\[CrossRef\]](#)
39. Tatsumi, M.; Yagi, Y.; Kadono, K.; Kaibara, K.; Iijima, M.; Ohishi, T.; Tanaka, H.; Hirata, T.; Mitchell, R. New Energy Efficient Processes and Improvements for Flue Gas CO₂ Capture. *Energy Procedia* **2011**, *4*, 1347–1352. [\[CrossRef\]](#)
40. Knudsen, J.N.; Jensen, J.N.; Vilhelmsen, P.J.; Biede, O. Experience with CO₂ Capture from Coal Flue Gas in Pilot-Scale: Testing of Different Amine Solvents. *Energy Procedia* **2009**, *1*, 783–790. [\[CrossRef\]](#)
41. Lemaire, E.; Bouillion, P.A.; Gomez, A.; Kittel, J.; Gonzalez, S.; Carrette, P.L.; Delfort, B.; Mongin, P.; Alix, P.; Normand, L. New IFP Optimized First Generation Process for Postcombustion Carbon Capture. *Energy Procedia* **2011**, *4*, 1361–1368. [\[CrossRef\]](#)
42. Gayheart, J.W.; Moorman, S.A.; Parsons, T.R.; Poling, C.W. Babcock & Wilcox Power Generation Group, Inc. RSATTM Process and Field Demonstration of the OptiCapTM Advanced Solvent at the US-DOE'S National Carbon Capture Center. *Energy Procedia* **2013**, *37*, 1951–1967. [\[CrossRef\]](#)
43. Monteiro, J.G.M.S.; Pinto, D.D.D.; Luo, X.; Knuutila, H.; Hussain, S.; Mba, E.; Hartono, A.; Svendsen, H.F. Activity-Based Kinetics of the Reaction of Carbon Dioxide with Aqueous Amine Systems. Case Studies: MAPA and MEA. *Energy Procedia* **2013**, *37*, 1888–1896. [\[CrossRef\]](#)
44. Pavlish, B.M.; Stanislawski, J.J.; Fiala, N.J.; Kay, J.P. Novel Solvent-Gas Contactor for CO₂ Capture Cost Reductions. *Energy Procedia* **2013**, *37*, 1941–1950. [\[CrossRef\]](#)
45. Olutoye, M.A.; Eterigho, E.J. Modelling of a Gas Absorption Column for CO₂-NaOH System under Unsteady-State Regime. *Leonardo Electron. J. Pract. Technol.* **2008**, *7*, 105–114.
46. Aouini, I.; Ledoux, A.; Estel, L.; Mary, S.; Grimaud, J.; Valognes, B. Study of Carbon Dioxide Capture from Industrial Incinerator Flue Gas on a Laboratory Scale Pilot. *Energy Procedia* **2011**, *4*, 1729–1736. [\[CrossRef\]](#)
47. Nielsen, P.T.; Li, L.; Rochelle, G.T. Piperazine Degradation in Pilot Plants. *Energy Procedia* **2013**, *37*, 1912–1923. [\[CrossRef\]](#)
48. Ohashi, Y.; Ogawa, T.; Suzuki, K. An Update of the Development of Carbon Dioxide Removal System from the Flue Gas of Coal Fired Power Plant in Toshiba. *Energy Procedia* **2013**, *37*, 1924–1932. [\[CrossRef\]](#)
49. Øi, L.E.; Lundberg, J.; Pedersen, M.; Hansen, P.M.; Melaaen, M.C. Laboratory Rig for Atmospheric CO₂ Absorption and Desorption under Pressure. *Energy Procedia* **2013**, *37*, 1933–1940. [\[CrossRef\]](#)
50. Razi, N.; Svendsen, H.F.; Bolland, O. The Impact of Design Correlations on Rate-Based Modeling of a Large Scale CO₂ Capture with MEA. *Energy Procedia* **2013**, *37*, 1977–1986. [\[CrossRef\]](#)

-
51. Mathias, P.M.; Reddy, S.; Smith, A.; Afshar, K. A Guide to Evaluate Solvents and Processes for Post-Combustion CO₂ Capture. *Energy Procedia* **2013**, *37*, 1863–1870. [[CrossRef](#)]
 52. Lim, Y.; Kim, J.; Jung, J.; Lee, C.S.; Han, C. Modeling and Simulation of CO₂ Capture Process for Coalbased Power Plant Using Amine Solvent in South Korea. *Energy Procedia* **2013**, *37*, 1855–1862. [[CrossRef](#)]

Disclaimer/Publisher’s Note: The statements, opinions and data contained in all publications are solely those of the individual author(s) and contributor(s) and not of MDPI and/or the editor(s). MDPI and/or the editor(s) disclaim responsibility for any injury to people or property resulting from any ideas, methods, instructions or products referred to in the content.